

# Realizing mechanical dynamical Casimir effect with low-frequency oscillator

Tian-hao Jiang<sup>1</sup> and Jun Jing<sup>1,\*</sup>

<sup>1</sup>*School of Physics, Zhejiang University, Hangzhou 310027, Zhejiang, China*

(Dated: August 6, 2024)

We realize the mechanical dynamical Casimir effect (DCE) in a hybrid optomechanical system consisting of a cavity mode, a low-frequency mechanical oscillator, and a two-level atomic system. Described by the effective Hamiltonian, the mechanical energy is found to be directly converted into the output photons through a three-wave-mixing mechanism. It is dramatically distinct from the quantum simulation of a parametric DCE in such as superconducting circuits. Using a master-equation approach, we analyze the system dynamics in various regimes with respect to the ratio of the effective coupling strength and the loss rate of the system. The dynamics under the strong-coupling regime confirms various three-wave-mixing process for creating photons by annihilation of the mechanical and atomic excitations. And that under the weak-coupling regime demonstrates the continuous production of photons by driving both mechanical oscillator and atom. By virtue of the two-level system, our method avoids the rigorous requirement for the high-frequency mechanical oscillator, that was demanded in standard DCE under the double-photon resonance. It is found that the mechanical frequency can be about two orders of magnitude smaller than the output photons.

## I. INTRODUCTION

The uncertainty principle in quantum mechanics leads to the vacuum state filled with constant activity. Quantum fluctuations within the vacuum give rise to a myriad of particles that appear to materialize and vanish in an instant [1–4]. Examples include the Schwinger effect [5], Hawking radiation [1, 6], Unruh effect [7], and the dynamical Casimir effect (DCE) [3, 8]. Proposed in about 1970 [9], DCE successfully predicted that a cavity with a moving mirror can lead to photon production when the mirror is twice of the cavity mode [10] in vibration frequency. DCE can be defined as a macroscopic phenomena resulting from the alterations of the quantum vacuum state due to the rapid changes in the boundary positions or properties that confine the fields [11].

Investigations about DCE have been extended from the cosmological problems, such as the particle creation due to the boundary motion that constrains the field in the curved space-time or in the presence of gravitational fields [12–15], to the quantum information field. For example, DCE can be used to cool down the cavity wall in the presence of a non-vanishing temperature gradient between the wall and the cavity [16]. A quantum Otto heat engine has been implemented with DCE [17], which operates within a cavity constructed by two oscillating mirrors confining an optical field. The mutual transformation between phonons and photons by DCE leads to an energy exchange between a cold bath and a hot bath, in which the walls and the field mode constitute collectively the working substance of the engine. Other applications on DCE include entanglement generation [18–22], quantum gates construction [23, 24], quantum steering [25], and quantum communication [26].

Direct realization of DCE challenges the current experiments [27] primarily due to the difficulty in altering

the boundary conditions of massive mirrors with a sufficiently high frequency. The double-photon resonant condition requires that the mechanical frequency  $\omega_m$  to be about twice the cavity mode  $\omega_c$  [10]. In another word, to produce the typical microwave photons of  $\omega_c \sim 5$  GHz through DCE, the frequency of the mechanical oscillator should be about  $\omega_m \sim 10$  GHz, which is much larger than that recently realized in experiments [28]. Another relevant challenge in optomechanical systems [29] is the high-frequency driving used to constantly excite the phonon mode. These problems have been addressed by the proposals for parametric dynamical Casimir effect (PDCE) [30–33], which suggest to simulate the boundary conditions by the effective motion. For example, microwave photons can emit from vacuum by fast modulation over the flux through the superconducting quantum-interference device [3, 30, 31, 34] or over the refraction index of a Josephson metamaterial [8].

While PDCE can simulate DCE in physics, they are not the direct observations. With respect to the essential feature of DCE, i.e., a direct conversion of the mechanical energy into the photon output, several methods are proposed to realize the mechanical dynamical Casimir effect (MDCE) [27, 29, 35–38]. For example, an amplified MDCE can be observed in the squeezed frame [27], which is realized by a detuned driving, under the resonant coupling between the mechanical oscillator and the squeezed cavity mode. Photons can be continuously generated by coupling the mechanical oscillator to a phononic reservoir with a finite temperature [37]. The standard condition about the double-photon resonance can be relaxed to  $k\omega_m = 2\omega_c$  with  $k$  integer by using an ultrastrong optomechanical coupling  $g/\omega_c \geq 0.1$  [29]. Although this relaxation indicates a significant advancement,  $k$  is severely limited. A substantial reduction in the mechanical frequency thus remains desired to the practical implementation of MDCE.

In this work, we propose to realize MDCE in a hybrid qubit-photon-phonon system, comprising of a cav-

\* Email address: jingjun@zju.edu.cn

ity with a movable mirror and a two-level system [39]. Using the effective Hamiltonian theory [40–42], we find that a three-wave-mixing process involving the annihilation of phonon and atomic excitations and the creation of microwave photons in the cavity, constitutes the underlying mechanism of MDCE. The system dynamics shows that MDCE can be realized in a much lower range of the mechanical frequency than the previous works. As the mechanical frequency decreases, our calculation about a signal-to-noise ratio distinguishes the photon production based on MDCE out of that based on the Rabi oscillation between the cavity mode and the qubit under driving. The role played by MDCE is found to be dominant even when the phonon frequency is as low as several percentages of the photon frequency.

The rest part of this paper is structured as following. In Sec. II, we describe the hybrid system and the full Hamiltonian. We obtain the parametric conditions for the three-wave-mixing process, which generates photon in the cavity and simultaneously annihilates atomic excitation and phonon. The relevant effective Hamiltonian is confirmed by comparing the analytical results and the numerical simulation. We discuss the population dynamics of photons, phonons, and qubit in the strong-coupling and the weak-coupling regimes in Secs. III A and III B, respectively. In Sec. III A, it is verified that the photon output is determined by the three-wave-mixing mechanism. In Sec. III B, a continuous output of photons is realized through continuous driving on the mechanical motion and qubit. We summarize the whole paper in Sec. IV.

## II. THEORETICAL MODEL

Consider a cavity optomechanical setup composed of three components: a cavity optical resonator, a mechanical oscillator, and a two-level atomic system (qubit). The full Hamiltonian is constructed by the free Hamiltonian and the interaction Hamiltonian.

$$H = H_0 + V. \quad (1)$$

The free Hamiltonian ( $\hbar = 1$ ) reads

$$H_0 = \omega_a \sigma_+ \sigma_- + \omega_c a^\dagger a + \omega_m b^\dagger b, \quad (2)$$

where the level splitting of the atom is  $\omega_a$  and the eigenfrequencies for photon and phonon are  $\omega_c$  and  $\omega_m$ , respectively.  $\sigma_+$  and  $\sigma_-$  are the raising and lowering operators, respectively, for the qubit.  $a$  ( $b$ ) and  $a^\dagger$  ( $b^\dagger$ ) are annihilation and creation operators for photon (phonon), respectively. The interaction Hamiltonian [39]  $V = V_{\text{AF}} + V_{\text{OM}} + V_{\text{DCE}}$  consists of the interaction between atom and cavity optical field  $V_{\text{AF}}$  and that between the cavity field and the mechanical mode  $V_{\text{OM}} + V_{\text{DCE}}$ , where  $V_{\text{OM}}$  and  $V_{\text{DCE}}$  are the photon-pressure term and the dynamical-Casimir-effect term, respectively. In par-

ticular, we have

$$\begin{aligned} V_{\text{AF}} &= \lambda(a^\dagger + a)(\sigma_+ + \sigma_-), \\ V_{\text{OM}} &= ga^\dagger a(b + b^\dagger), \\ V_{\text{DCE}} &= \frac{g}{2}(a^2 + a^{\dagger 2})(b + b^\dagger). \end{aligned} \quad (3)$$

where  $\lambda$  is the coupling strength between the two-level atom and the cavity mode and  $g$  denotes the optomechanical coupling strength. Most optomechanical models neglected the DCE interaction between photon and phonon [43–45]. This approximation holds when the mechanical frequency is significantly smaller than the cavity frequency [46].

The fundamental mechanism in our method for MDCE is based on the three-wave-mixing process involving the three components of the whole system, that can be described by an effective Hamiltonian based on the second-order perturbation theory. The eigenstates for the unperturbed Hamiltonian  $H_0$  can be expressed by the tensor-product state  $|jnm\rangle \equiv |j\rangle \otimes |n\rangle \otimes |m\rangle$ , where  $|j\rangle$ ,  $j = g, e$ , labels the atom state and  $|n\rangle$  ( $|m\rangle$ ) denotes the number state of the cavity mode (mechanical mode). The dynamic transition, which is in charge of the photon generation by the deexcitation of atom and phonon, occurs between the states  $|e, n, m + 1\rangle$  and  $|g, n + 1, m\rangle$ .

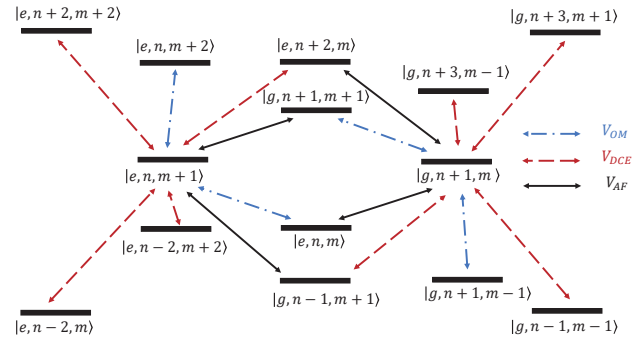


FIG. 1. All the second-order transition paths linking the target eigenstate  $|e, n, m + 1\rangle$  and  $|g, n + 1, m\rangle$ . Blue dot-dashed lines mark the transitions induced by the standard optomechanical interaction  $V_{\text{OM}}$ . Red dashed lines mark those by the DCE interaction  $V_{\text{DCE}}$ . Black solid lines mark the contribution from the atom-field interaction  $V_{\text{AF}}$ .

The effective Hamiltonian spanned by  $\{|e, n, m + 1\rangle, |g, n + 1, m\rangle\}$  for arbitrary  $n$  and  $m$  can be extracted from the full Hamiltonian. The interaction Hamiltonian  $V$  is regarded as a perturbation. The effective coupling strength or energy shift between any eigenstates  $|i\rangle$  and  $|f\rangle$  of unperturbed Hamiltonian  $H_0$  can be obtained by

$$\Omega = V_{fi} + \sum_{n \neq i, f} \frac{V_{fn} V_{ni}}{\omega_i - \omega_n}, \quad (4)$$

where  $V_{nm} \equiv \langle n | V | m \rangle$  and  $\omega_n$  is the eigenenergy of eigenstate  $|n\rangle$  under  $H_0$ . When  $i \neq f$ , Eq. (4) quantifies their

coupling strength. Otherwise, it gives rise to the energy-level shift or correction  $\epsilon$ .

Figure 1 demonstrates the transition paths connecting the two target eigenstates  $\{|e, n, m+1\rangle, |g, n+1, m\r\rangle\}$  and the round trips for them, which can be used to calculate the effective coupling strength and the energy-level shift, respectively. By setting the initial state  $|i\rangle = |e, n, m+1\rangle$  and the final state  $|f\rangle = |g, n+1, m\r\rangle$  in Eq. (4) and summarizing the contributions from the four paths mediated by  $|e, n+2, m\rangle$ ,  $|g, n+1, m+1\r\rangle$ ,  $|e, n, m\r\rangle$ , and  $|g, n-1, m+1\r\rangle$ , one can obtain the expression of the effective coupling strength  $g_{\text{eff}}$ :

$$g_{\text{eff}} = -g\lambda\sqrt{n+1}\sqrt{m+1}\left(\frac{1}{2\omega_c - \omega_m} + \frac{1}{\omega_m}\right). \quad (5)$$

It can be verified that  $V_{\text{DCE}}$  contributes to the first term in Eq. (5),  $V_{\text{OM}}$  contributes to the second term, and  $V_{\text{AF}}$  contributes to both of them.

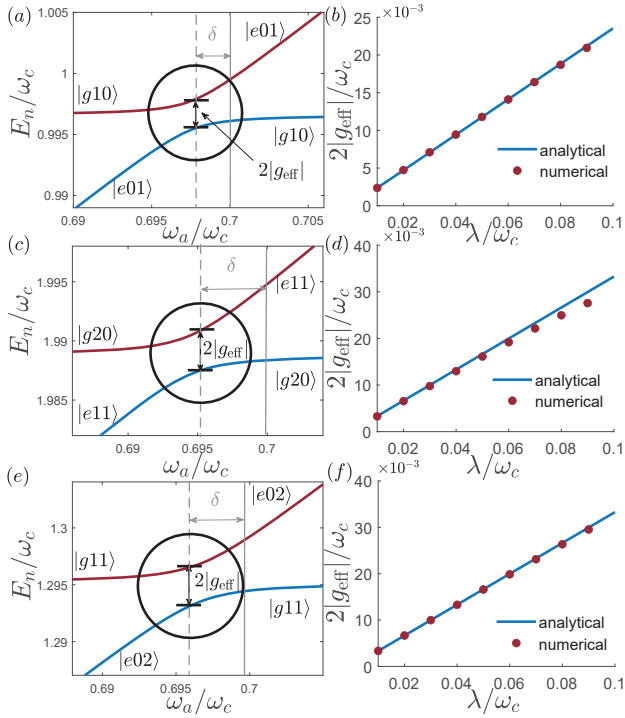


FIG. 2. (a), (c), (e): Energy levels and avoided level crossings for various three-wave-mixing processes as functions of the qubit transition frequency  $\omega_a$ .  $\omega_m = 0.3\omega_c$ ,  $g = 0.03\omega_c$ , and  $\lambda = 0.01\omega_c$ . (b), (d), (f): Comparison between the numerical evaluation of the normalized effective coupling strengths (red dots) and the corresponding analytical results (blue solid line).  $\omega_m = 0.3\omega_c$ ,  $\omega_a = 0.7\omega_c$ , and  $g = 0.03\omega_c$ .

In Fig. 2, we demonstrate the avoided level crossings (distinguished by the dark circles) describing transitions between various initial and final states in the diagrams of energy levels  $\{E_n\}$  for the full Hamiltonian. In particular, Figs. 2(a), (c), and (e) plot the target state pairs  $|g10\rangle \leftrightarrow |e01\rangle$ ,  $|g20\rangle \leftrightarrow |e11\rangle$ , and  $|g11\rangle \leftrightarrow |e02\rangle$ , respectively. The eigenvalues, which vary with  $\omega_a$ , are obtained

by a standard numerical diagonalization method in a truncated Hilbert space of the full Hamiltonian. Around the three-wave-mixing condition, i.e.,  $\omega_a + \omega_m = \omega_c$ , the two states  $|e, n, m+1\r\rangle$  and  $|g, n+1, m\r\rangle$  become nearly degenerate and the avoided level crossing occurs with a splitting given by the effective coupling strength in Eq. (4). A perfect Rabi oscillation with a transition rate  $2|g_{\text{eff}}|$  can be observed between  $|e, n, m+1\r\rangle$  and  $|g, n+1, m\r\rangle$  as long as the energy shift  $\delta$  is exactly obtained. For our method, that oscillation implies that the qubit facilitates the conversion of phonon energy to photon.

And Figs. 2(b), (d), and (f) are used to verify the effective coupling strength  $g_{\text{eff}}$  in Eq. (5), which is based on the second-order perturbation in Eq. (4), in terms of the range of the coupling strength  $\lambda$  between qubit and cavity mode. It is shown that the analytical results do match with the numerical ones even when the normalized qubit-photon interaction strength is close to the regime  $\lambda/\omega_c \leq 0.1$ . Nevertheless, such an ultrastrong coupling is not required in our method of realizing MDCE.

The energy shift  $\delta$  (distinguished by the gray dashed and solid lines) is clearly caused by the interaction Hamiltonian  $V$ . Similar to the effective coupling strength  $g_{\text{eff}}$ , it can be well explained by the second-order perturbation theory in Eq. (4). One can obtain the energy shifts  $\epsilon_1$  and  $\epsilon_2$  for the two target states,  $|g, n+1, m\r\rangle$  and  $|e, n, m+1\r\rangle$ , respectively. Summarizing all the eight paths in Fig. 1 starting from  $|g, n+1, m\r\rangle$ , passing a mediated state, and then going back to  $|g, n+1, m\r\rangle$ , one can obtain the energy shift up to the second order of  $g$  and  $\lambda$ :

$$\epsilon_1 = -\frac{1}{4}g^2\left(\frac{n^2 + 4nm + 5n + 6m + 6}{2\omega_c + \omega_m} + \frac{-n^2 + 4nm + 6m - n}{2\omega_c - \omega_m}\right) - \frac{(n+2)\lambda^2}{\omega_c + \omega_a} - \frac{(n+1)\lambda^2}{\omega_a - \omega_c} - \frac{(n+1)^2g^2}{\omega_m}. \quad (6)$$

Similarly, the energy shift for the state  $|e, n, m+1\r\rangle$  reads,

$$\epsilon_2 = -\frac{1}{4}g^2\left(\frac{2n^2 + 4nm + 6n + 2m + 4}{2\omega_c + \omega_m} + \frac{-n^2 + 4nm + 2m + 5n + 2}{2\omega_c - \omega_m}\right) + \frac{n\lambda^2}{\omega_c + \omega_a} - \frac{(n+1)\lambda^2}{\omega_c - \omega_a} - \frac{n^2g^2}{\omega_m}. \quad (7)$$

Equations (5), (6), and (7) give rise to the effective Hamiltonian in the subspace spanned by  $\{|e, n, m+1\r\rangle, |g, n+1, m\r\rangle\}$ :

$$\begin{aligned} H_{\text{eff}} = & g_{\text{eff}}(|e, n, m+1\rangle\langle g, n+1, m| + \text{H.c.}) \\ & + E_g|g, n+1, m\r\rangle\langle g, n+1, m| \\ & + E_e|e, n, m+1\r\rangle\langle e, n, m+1|, \end{aligned} \quad (8)$$

where  $E_g = (n+1)\omega_c + m\omega_m + \epsilon_1$  and  $E_e = \omega_a + n\omega_c + (m+1)\omega_m + \epsilon_2$  are the eigenenergies for  $|g, n+1, m\r\rangle$

and  $|e, n, m+1\rangle$ , respectively. To realize a perfect Rabi oscillation between the two states, the last two terms in Eq. (8) should become the identity operator in the corresponding subspace. Thus the resonant condition  $E_g = E_e$ , i.e.,  $\omega_c + \epsilon_1 = \omega_a + \omega_m + \epsilon_2$ , yields the energy shift  $\delta$  for the avoided level crossings in Fig. 2:

$$\begin{aligned} \delta &\equiv \epsilon_2 - \epsilon_1 = \omega_c - \omega_m - \omega_a \\ &= \frac{g^2}{4} \left( \frac{-n^2 - n + 4m + 2}{2\omega_c + \omega_m} + \frac{-6n + 4m - 2}{2\omega_c - \omega_m} \right) \\ &+ \frac{2(n+1)\lambda^2}{\omega_a - \omega_c} + \frac{(2n+1)g^2}{\omega_m} + \frac{2(n+1)\lambda^2}{\omega_a + \omega_c}. \end{aligned} \quad (9)$$

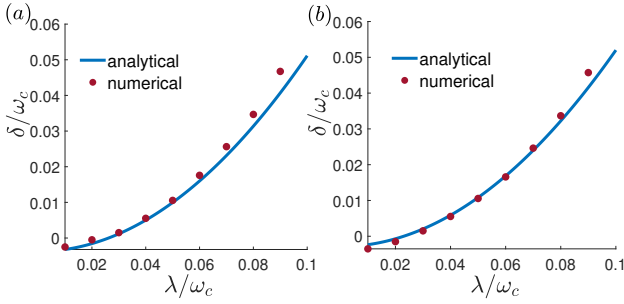


FIG. 3. Comparison between the numerically (red dots) calculated normalized energy shift  $\delta/\omega_c$  and the corresponding analytical results (blue solid line). The transitions in (a) and (b) are  $|g10\rangle \leftrightarrow |e01\rangle$  and  $|g11\rangle \leftrightarrow |e02\rangle$ , respectively. The parameters are the same as Fig. 2.

In Figs. 3(a) and (b), we compare the analytical results and the numerical evaluation obtained by Eq. (9) for the energy shift in the transitions of  $|g10\rangle \leftrightarrow |e01\rangle$  and  $|g11\rangle \leftrightarrow |e02\rangle$ , respectively. The calculations are performed under the same condition as Fig. 2. It is shown that the analytical results for energy shift also do match with the numerical ones when the normalized qubit-photon interaction strength  $\lambda/\omega_c \leq 0.1$ . In this case, the effective Hamiltonian (8) can be expressed as

$$H_{\text{eff}} \approx g_{\text{eff}} (|e, n, m+1\rangle \langle g, n+1, m| + \text{H.c.}) \quad (10)$$

The three-wave-mixing process described by the effective Hamiltonian provides the main mechanism for MDCE emerging in the system dynamics provided in the following section. It can be witnessed by the Fourier transform about the mean photon number in Sec. III A, where each Fourier peak reveals a transition between distinct pair of target states.

### III. SYSTEM DYNAMICS

In this section, we explore the system dynamics under the external driving on the mechanical oscillator and the qubit, which is necessary to constantly generate photons in the cavity in coordination with the three-wave-mixing

process supported by the effective Hamiltonian (10). The driving Hamiltonian  $H_d(t)$  can be written as

$$H_d(t) = F_1(t)(b^\dagger + b) + F_2(t)(\sigma_+ + \sigma_-), \quad (11)$$

where  $F_1(t)$  and  $F_2(t)$  describe the external force or modulation applied to the movable mirror and qubit, respectively. Here  $F_1(t)$  and  $F_2(t)$  are assumed to follow the same formation and distinct only in the driving frequency.

We employ a Lindblad master equation to evaluate the density-matrix operator  $\rho(t)$  of the system under a zero-temperature dissipative environment. It is given by

$$\begin{aligned} \dot{\rho}(t) &= i[\rho(t), H + H_d(t)] + \kappa \mathcal{L}[\sigma_-]\rho(t) \\ &+ \eta \mathcal{L}[a]\rho(t) + \gamma \mathcal{L}[b]\rho(t), \end{aligned} \quad (12)$$

where  $\kappa$ ,  $\eta$ , and  $\gamma$  are the atomic, photonic, and mechanical loss rates, respectively. And the superoperator  $\mathcal{L}$  is defined as

$$\mathcal{L}[o]\rho \equiv \frac{1}{2} (2O\rho O^\dagger - O^\dagger O\rho - \rho O^\dagger O), \quad (13)$$

$$O \equiv \sum_{E_n > E_m} \langle \Psi_m | (o + o^\dagger) | \Psi_n \rangle | \Psi_m \rangle \langle \Psi_n | \quad (14)$$

where  $o = \sigma_-, a, b$  and  $|\Psi_n\rangle$  are the eigenvectors of the full Hamiltonian  $H$  (1).

In numerical simulations, the whole system is assumed to be initialized as the ground state  $|000\rangle$ . The system parameters follow the setting in Fig. 2(a), i.e., the mechanical frequency  $\omega_m = 0.3\omega_c$ , the atomic splitting  $\omega_a \approx 0.7\omega_c - \delta$ , the qubit-photon coupling strength  $\lambda = 0.01\omega_c$ , and the photon-phonon coupling strength  $g = 0.03\omega_c$ , unless otherwise stated. Substituting them into Eq. (5), the effective coupling strength is found to be  $|g_{\text{eff}}| = 1.18 \times 10^{-3}\omega_c$ .

In the following, we will study the system dynamics in the strong-coupling and weak-coupling regimes when the effective coupling strength  $|g_{\text{eff}}|$  is larger or smaller than the system loss rate, respectively. With respect to MDCE, the former case is used to distinguish the underlying mechanism. And the latter case is used to investigate the frequency range of the mechanical oscillator in our method, which is meaningful to avoid the high-frequency requirement in both eigen-frequency and driving frequency for the mechanical oscillator.

In Sec. III A, an ultra-fast drive, which is nearly an instant pulse, is used to rapidly excite the mechanical oscillator and the atom. Then approximately the system is mainly subject to the time-independent effective Hamiltonian in the subsequent time evolution. And the three-wave-mixing process is not severely influenced by the comparatively weak dissipation. In contrast, Sec. III B applies a continuous drive and a comparatively strong dissipation to realize MDCE with a low-frequency mechanical oscillator. To confirm that the photon output is essentially generated via a significant DCE rather than by the direct conversion from qubit to photon, we compare two scenarios: i.e., simultaneously driving the mechanical oscillator and the qubit and only driving the qubit.

### A. Strong-coupling regime

For the system dynamics in the strong-coupling regime, we set the loss rates as  $\kappa = \eta = \gamma = 10^{-4}\omega_c$  in the master equation (12). Thereby the effective coupling strength overwhelms the system loss and then one can observe the basic transition determined by the system Hamiltonian during the weak dissipative evolution. The two ultra-fast resonant pulses in Eq. (11) are set as

$$\begin{aligned} F_1(t) &= AG(t - t_0) \cos(\omega_m t), \\ F_2(t) &= AG(t - t_0) \cos(\omega_a t), \end{aligned} \quad (15)$$

respectively, where  $A$  is a dimensionless pulse amplitude or intensity. Here we use a compact Gaussian function to constrain the practical time extension of the pulse

$$G(t - t_0) = \frac{1}{\sqrt{2\pi}\sigma} \exp\left[-\frac{(t - t_0)^2}{2\sigma^2}\right], \quad (16)$$

where  $\sigma$  is the standard deviation and  $t_0$  is the central time point. They are fixed as  $\sigma = (16|g_{\text{eff}}|)^{-1}$  and  $t_0 = 100/\omega_c$ , respectively.

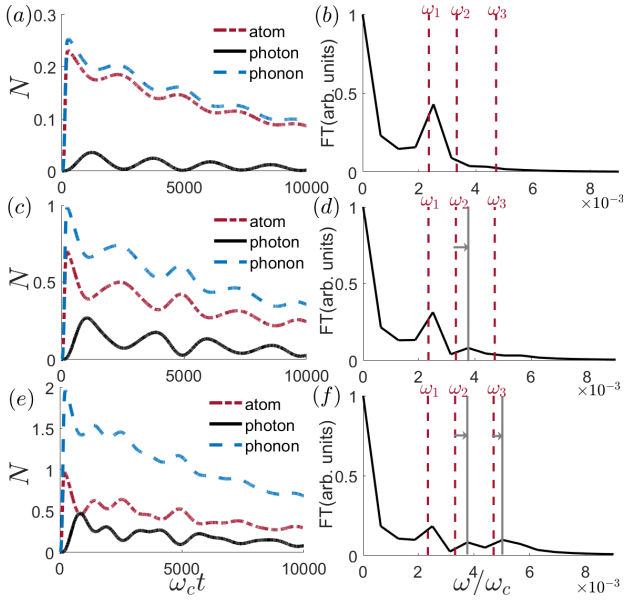


FIG. 4. Time evolution of the average population of the atom (red dot-dashed line), the mechanical oscillator (blue dotted line), and the cavity mode (black solid line) under the ultra-fast pulse in Eq. (15) with various intensity: (a)  $A = \pi/3$ , (c)  $A = 2\pi/3$ , (e)  $A = \pi$ . (b), (d), (f): Fourier transformation over the average photon number in (a), (c), and (e), respectively.

Figure 4 shows the evolution of the average excitation numbers of three components and the Fourier transformation of the mean photon number under different pulse amplitudes. The Fourier transformation can be defined by

$$F(\omega) = \sum_{k=0}^{M-1} N(k\Delta t) e^{-i\frac{2\pi}{M}\omega k\Delta t}, \quad (17)$$

where  $N$  is the mean photon number,  $\Delta t$  is the sampling time interval, and  $M$  is the sampling number of the mean photon number during the evolution.

In Fig. 4(a), the mechanical oscillator and the atom are rapidly excited on the pulse arrival. And the photon excitation is clearly delayed by a period of time. After a short-time interval according to the Gaussian amplitude in Eq. (16), the driving intensity reduces to nearly zero, resulting the subsequent dynamics is mainly determined by the full Hamiltonian  $H$  (1) or the effective Hamiltonian (10). The populations of the photon and the atom and the mean number of the photon manifest a complementary pattern in a sinusoidal-like evolution. In another word, the phonon number of the oscillator is in phase with the atomic excitation number and they are out of phase with the photon number. Confirmed by the Fourier analysis in Fig. 4(b), it is found that the excitation or energy transfer between the photon and the atom plus the phonon can be roughly described by the effective Hamiltonian

$$H_{\text{eff}} = g_{\text{eff}} (|e01\rangle\langle g10| + |g10\rangle\langle e01|), \quad (18)$$

with a transfer rate

$$\omega_1 = |g_{\text{eff}}| = g\lambda \left( \frac{1}{2\omega_c - \omega_m} + \frac{1}{\omega_m} \right). \quad (19)$$

It is evident that a peak around  $\omega_1$  is distinguished in the frequency domain.

As the driving intensity  $A$  increases, the mechanical oscillator can be populated to higher Fock states. The population dynamics in Fig. 4(c) and Fig. 4(e) then deviate gradually from the sinusoidal-like oscillation. It means that the dynamics becomes involving with multiple oscillations of various frequency. In regard of the photon generation, an extra three-wave-mixing process with higher Fock states, e.g.,  $|e02\rangle$  and  $|e11\rangle$ , can present in addition to that in Eq. (18).

When  $A = 2\pi/3$ , Fig. 4(d) suggests that the transitions  $|g20\rangle \leftrightarrow |e11\rangle$  and  $|g11\rangle \leftrightarrow |e02\rangle$  of the same transition frequency  $\omega_2$  become significant in dynamics. These two photon-generation channels or Rabi oscillations can be described by the following effective Hamiltonian:

$$H_{\text{eff}} \approx \omega_2 (|e11\rangle\langle g20| + |g20\rangle\langle e11|), \quad (20a)$$

$$H_{\text{eff}} \approx \omega_2 (|e02\rangle\langle g11| + |g11\rangle\langle e02|), \quad (20b)$$

where  $\omega_2 = \sqrt{2}\omega_1$  can be obtained by Eq. (5) with  $n = 1$  and  $m = 0$  or  $n = 0$  and  $m = 1$ . In comparison to Fig. 4(b), an extra peak presents around  $\omega_2$  in Fig. 4(d). A nonnegligible distance exists between the numerical simulation and the analytical result for  $\omega_2$ , which is partially due to the fact that the setting about the energy shift in Eq. (9) is state dependent. The resonant condition for  $|g10\rangle \leftrightarrow |e01\rangle$  in the effective Hamiltonian (18) is not suitable to Eqs. (20a) and (20b). It renders that the practical oscillation frequency is larger than  $\omega_2$ . This discussion also applies to the next peak frequency  $\omega_3$  in Fig. 4(f).

Similarly, in Fig. 4(f) with  $A = \pi$ , the Rabi oscillations  $|g21\rangle \leftrightarrow |e12\rangle$  ( $|g13\rangle \leftrightarrow |e04\rangle$ ,  $|g40\rangle \leftrightarrow |e31\rangle$ ) become distinguished underlying the population dynamics, although the transitions between lower Fock states still dominate. In comparison to Figs. 4(b) and 4(d), the extra oscillations in Fig. 4(f) are characterized with the transition frequency  $\omega_3 = 2\omega_1$ , which can be obtained by Eq. (5) with  $n = 1(0, 3)$  and  $m = 1(3, 0)$ .

## B. Weak-coupling regime

In Sec. III A, we have demonstrated that the three-wave-mixing process by the effective Hamiltonian (10) constitutes the main component during the system dynamics as well as the mechanism of converting the energy of the mechanical oscillator and atomic excitation into photons. In this section, to keep producing photons during the time evolution, the driving functions in Eq. (11) are modified to be

$$\begin{aligned} F_1(t) &= A\gamma \cos(\omega_m t), \\ F_2(t) &= A\gamma \cos(\omega_a t), \end{aligned} \quad (21)$$

where the drive intensity is set as  $A = 12$ . And we set the loss rate in the master equation (12) as  $C = \kappa = \eta = 10\gamma = 2.5 \times 10^{-3}\omega_c$  to ensure that the effective coupling strength now becomes smaller than the system loss, i.e.,  $|g_{\text{eff}}|/C < 1$ .

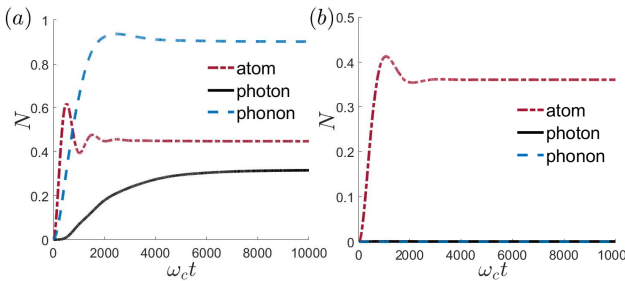


FIG. 5. Time evolution of the average population of the atom (red dot-dashed line), the mechanical oscillator (blue dotted line), and the cavity mode (black solid line) under the driving in Eq. (21). (a): both the mechanical oscillator and the atom are under driving; (b): Only the atomic driving is on.

Figure 5(a) shows that the average populations of both mechanical oscillator and atom rapidly arise under the continuous driving. After a time delay, the photon population starts increasing with a comparatively small rate. It is evident that the photon excitation comes from the phonon and atom in the three-wave mixing process after the latter two are sufficiently populated through external driving. By definition, MDCE can be observed after  $\omega_c t \approx 5000$  when the three components approach steady states, as a balance between the two driving and system dissipation. The photon population in the cavity is stabilized as 0.31, which is much larger than the current result in Ref. [27], where a detuned two-photon

driving is employed to squeeze the cavity mode in the optomechanical system. The coupling between the mechanical oscillator and the squeezed cavity mode leads to the amplification of MDCE. Under the same parametric setting, it is found that a cavity with a typical linewidth of  $\gamma/2\pi = 2$  MHz could emit  $3.8 \times 10^6$  photons per second by our method. Evidently, it can be detectable in current experiments. To confirm that photons in the cavity are practically generated by the vibration of mechanical oscillators, we switched off the mechanical driving in Fig. 5(b). The population dynamics of the three components show that the average photon number in the steady state is nearly vanishing.

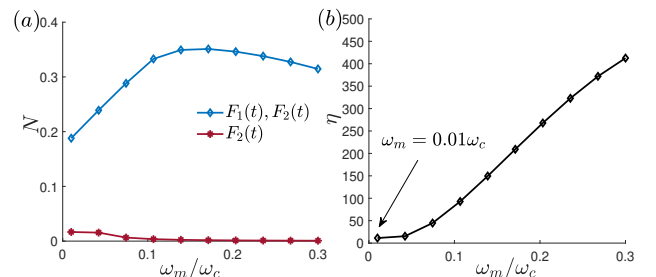


FIG. 6. (a) Stable photon number in the cavity as a function of the frequency of the mechanical oscillator under both atomic and mechanical driving (blue solid line marked with diamond) and under only atomic driving (red solid line marked with asterisk). (b) Signal-to-noise ratio between the photon generated by three-wave mixing process and that by the photon-atom Rabi oscillation as a function of the mechanical frequency.

Note that the parametric setting in Fig. 5 is the same as Fig. 2(a), where the mechanical frequency is about one order smaller than the output photon, i.e.,  $\omega_m = 0.3\omega_c$ . In practice, our method for realizing MDCE is extendable to a wide range for the low-frequency mechanical oscillator. In Fig. 6(a), we present the photon population of the steady state from  $\omega_m = 0.01\omega_c$  to  $\omega_m = 0.3\omega_c$  on either simultaneous driving both mechanical oscillator and qubit or only driving the qubit. These two cases demonstrate a similar distinction as that in Fig. 5. Through driving both components, the excited phonon and atomic excitation can be constantly used to generate photon, resulting in a detectable photon output. The stable population of photons in the cavity is not much sensitive to  $\omega_m$ . It is about 0.19 when  $\omega_m$  is as small as  $0.01\omega_c$ . And then it increases gradually with the frequency of the mechanical oscillator, until attains a peak value about 0.35 around  $\omega_m \approx 0.15\omega_c$ . It means that in such a wide range of  $\omega_m$ , the three-wave mixing process remains the basic mechanism underlying the system dynamics, as long as the atomic frequency can be adjusted accordingly to meet the condition  $\omega_c \approx \omega_a + \omega_m$ . However, one can also find that a nonvanishing photon generation only on driving the qubit, when  $\omega_m$  decreases to be less than about  $0.07\omega_c$  (see the red solid line marked with asterisk). It might be interpreted as a direct conversion between pho-

ton and atomic excitation, constituting a second resource of photon in addition to the three-wave mixing. A subsequent question is whether or not the result is still a MDCE when we employ a low-frequency mechanical oscillator in this hybrid system.

In Fig. 6(b), a signal-to-noise ratio is evaluated to identify the actual source of the photons, which is defined as  $\eta \equiv N_1/N_2$ . Here  $N_1$  and  $N_2$  are denoted as the steady-state numbers of signal photons and noisy photons generated by the three-wave mixing process involving the mechanical oscillator and through the Rabi oscillation between the atom and the cavity mode, respectively. The ratio is found to be a monotonically increasing function as the mechanical frequency. Even when  $\omega_m = 0.01\omega_c$ ,  $\eta$  is still over 11. Therefore, it is confirmed that our method allows to realize MDCE with a low-frequency mechanical oscillator. In comparison to the previous method [29] based on a multiple-phonon process  $k\omega_m = 2\omega_c$ , the frequency requirements of the mechanical oscillator as well as the driving frequency under the resonant condition can be reduced by at least two orders in magnitude. Also the photon-phonon coupling strength is not in an ultrastrong regime. Our method is accessible in current experiments, e.g., in Ref. [47], where the mechanical oscillator frequency is about  $\omega_m/2\pi \sim 65$  MHz, the cavity

frequency  $\omega_c/2\pi \sim 5$  GHz, and the radiation-pressure coupling between photon and phonon is up to 100 MHz.

#### IV. CONCLUSION

In this work, we have introduced a method for realizing instead of simulating the mechanical dynamical Casimir effect within a hybrid qubit-photon-phonon system. Our method yields appreciable photons in the cavity optomechanical system with a low-frequency mechanical oscillator, that greatly reduces the experimental cost in current platforms. Through an effective Hamiltonian based on the quantum-mechanical description of both the cavity field and the movable mirror, we identify that the three-wave-mixing process inherent in the system dynamics constitutes the fundamental mechanism for MDCE. The relevant transitions for creating photons through de-exciting the atom and mechanical oscillator provide a pathway for detecting MDCE in the steady state under continuous driving and weak dissipation. We also use a signal-to-noise ratio to confirm that the output photon is a truly result from MDCE rather than from the Rabi oscillation between atom and photon. Our work pushes the mechanical DCE into the low-frequency regime for mechanical oscillator.

---

[1] S. W. Hawking, *Black hole explosions?* *Nature (London)* **248**, 30 (1974).

[2] J. Schwinger, *Casimir light: The source.* *Proc. Natl. Acad. Sci. USA* **90**, 2105 (1993).

[3] C. M. Wilson, G. Johansson, A. Pourkabirian, M. Simoen, J. R. Johansson, T. Duty, F. Nori, and P. Delsing, *Observation of the dynamical casimir effect in a superconducting circuit*, *Nature (London)* **479**, 376 (2011).

[4] O. Di Stefano, A. Settineri, V. Macrì, A. Ridolfo, R. Stassi, A. F. Kockum, S. Savasta, and F. Nori, *Interaction of mechanical oscillators mediated by the exchange of virtual photon pairs*, *Phys. Rev. Lett.* **122**, 030402 (2019).

[5] J. Schwinger, *On gauge invariance and vacuum polarization*, *Phys. Rev.* **82**, 664 (1951).

[6] S. W. Hawking, *Particle creation by black holes*, *Commun. Math. Phys.* **43**, 199 (1975).

[7] W. G. Unruh, *Notes on black-hole evaporation*, *Phys. Rev. D* **14**, 870 (1976).

[8] P. Lähteenmäki, G. S. Paraoanu, J. Hassel, and P. J. Hakonen, *Dynamical casimir effect in a josephson metamaterial*, *Proc. Natl. Acad. Sci. U.S.A.* **110**, 4234 (2013).

[9] G. T. Moore, *Quantum theory of the electromagnetic field in a variable-length one-dimensional cavity*, *J. Math. Phys.* **11**, 2679 (2003).

[10] A. Lambrecht, M.-T. Jaekel, and S. Reynaud, *Motion induced radiation from a vibrating cavity*, *Phys. Rev. Lett.* **77**, 615 (1996).

[11] V. Dodonov, *Fifty years of the dynamical casimir effect*, *Physics* **2**, 67 (2020).

[12] I. Brevik, K. A. Milton, S. D. Odintsov, and K. E. Osetrin, *Dynamical casimir effect and quantum cosmology*, *Phys. Rev. D* **62**, 064005 (2000).

[13] M. Ruser and R. Durrer, *Dynamical casimir effect for gravitons in bouncing braneworlds*, *Phys. Rev. D* **76**, 104014 (2007).

[14] M. P. E. Lock and I. Fuentes, *Dynamical casimir effect in curved spacetime*, *New J. Phys.* **19**, 073005 (2017).

[15] A. Ottewill and S. Takagi, *Radiation by moving mirrors in curved space-time*, *Prog. Theor. Phys.* **79**, 429 (1988).

[16] A. Ferreri, D. E. Bruschi, F. K. Wilhelm, F. Nori, and V. Macrì, *Phonon-photon conversion as mechanism for cooling and coherence transfer*, *Phys. Rev. Res.* **6**, 023320 (2024).

[17] A. Ferreri, V. Macrì, F. K. Wilhelm, F. Nori, and D. E. Bruschi, *Quantum field heat engine powered by phonon-photon interactions*, *Phys. Rev. Res.* **5**, 043274 (2023).

[18] S. Felicetti, M. Sanz, L. Lamata, G. Romero, G. Johansson, P. Delsing, and E. Solano, *Dynamical casimir effect entangles artificial atoms*, *Phys. Rev. Lett.* **113**, 093602 (2014).

[19] X. Busch, R. Parentani, and S. Robertson, *Quantum entanglement due to a modulated dynamical casimir effect*, *Phys. Rev. A* **89**, 063606 (2014).

[20] C. Aron, M. Kulkarni, and H. E. Türeci, *Steady-state entanglement of spatially separated qubits via quantum bath engineering*, *Phys. Rev. A* **90**, 062305 (2014).

[21] D. Z. Rossatto, S. Felicetti, H. Eneriz, E. Rico, M. Sanz, and E. Solano, *Entangling polaritons via dy-*

namical casimir effect in circuit quantum electrodynamics, *Phys. Rev. B* **93**, 094514 (2016).

[22] A. Agustí, E. Solano, and C. Sabín, *Entanglement through qubit motion and the dynamical casimir effect*, *Phys. Rev. A* **99**, 052328 (2019).

[23] N. Friis, M. Huber, I. Fuentes, and D. E. Bruschi, *Quantum gates and multipartite entanglement resonances realized by nonuniform cavity motion*, *Phys. Rev. D* **86**, 105003 (2012).

[24] D. E. Bruschi, A. Dragan, A. R. Lee, I. Fuentes, and J. Louko, *Relativistic motion generates quantum gates and entanglement resonances*, *Phys. Rev. Lett.* **111**, 090504 (2013).

[25] C. Sabín and G. Adesso, *Generation of quantum steering and interferometric power in the dynamical casimir effect*, *Phys. Rev. A* **92**, 042107 (2015).

[26] G. Benenti, A. D'Arrigo, S. Siccaldi, and G. Strini, *Dynamical casimir effect in quantum-information processing*, *Phys. Rev. A* **90**, 052313 (2014).

[27] W. Qin, V. Macrì, A. Miranowicz, S. Savasta, and F. Nori, *Emission of photon pairs by mechanical stimulation of the squeezed vacuum*, *Phys. Rev. A* **100**, 062501 (2019).

[28] A. D. O'Connell, M. Hofheinz, M. Ansmann, R. C. Bialczak, M. Lenander, E. Lucero, M. Neeley, D. Sank, H. Wang, M. Weides, J. Wenner, J. M. Martinis, and A. N. Cleland, *Quantum ground state and single-phonon control of a mechanical resonator*, *Nature (London)* **464**, 697 (2010).

[29] V. Macrì, A. Ridolfo, O. Di Stefano, A. F. Kockum, F. Nori, and S. Savasta, *Nonperturbative dynamical casimir effect in optomechanical systems: Vacuum casimir-rabi splittings*, *Phys. Rev. X* **8**, 011031 (2018).

[30] J. R. Johansson, G. Johansson, C. M. Wilson, and F. Nori, *Dynamical casimir effect in a superconducting coplanar waveguide*, *Phys. Rev. Lett.* **103**, 147003 (2009).

[31] J. R. Johansson, G. Johansson, C. M. Wilson, and F. Nori, *Dynamical casimir effect in superconducting microwave circuits*, *Phys. Rev. A* **82**, 052509 (2010).

[32] M. Crocce, D. A. R. Dalvit, F. C. Lombardo, and F. D. Mazzitelli, *Model for resonant photon creation in a cavity with time-dependent conductivity*, *Phys. Rev. A* **70**, 033811 (2004).

[33] P. D. Nation, J. R. Johansson, M. P. Blencowe, and F. Nori, *Colloquium : Stimulating uncertainty: Amplifying the quantum vacuum with superconducting circuits*, *Rev. Mod. Phys.* **84**, 1 (2012).

[34] V. V. Dodonov, *Current status of the dynamical casimir effect*, *Phys. Scr.* **82**, 038105 (2010).

[35] E. Sassaroli, Y. N. Srivastava, and A. Widom, *Photon production by the dynamical casimir effect*, *Phys. Rev. A* **50**, 1027 (1994).

[36] J. Haro and E. Elizalde, *Hamiltonian approach to the dynamical casimir effect*, *Phys. Rev. Lett.* **97**, 130401 (2006).

[37] A. Settineri, V. Macrì, L. Garziano, O. Di Stefano, F. Nori, and S. Savasta, *Conversion of mechanical noise into correlated photon pairs: Dynamical casimir effect from an incoherent mechanical drive*, *Phys. Rev. A* **100**, 022501 (2019).

[38] Z.-L. Lan, Y.-W. Chen, L.-Y. Cheng, L. Chen, S.-Y. Ye, and Z.-R. Zhong, *Dynamical casimir effect in a hybrid cavity optomechanical system*, *Quantum Inf. Process.* **23**, 72 (2024).

[39] B. Wang, J.-M. Hu, V. Macrì, Z.-L. Xiang, and F. Nori, *Coherent resonant coupling between atoms and a mechanical oscillator mediated by cavity-vacuum fluctuations*, *Phys. Rev. Research* **5**, 013075 (2023).

[40] L. Garziano, V. Macrì, R. Stassi, O. Di Stefano, F. Nori, and S. Savasta, *One photon can simultaneously excite two or more atoms*, *Phys. Rev. Lett.* **117**, 043601 (2016).

[41] V. Macrì, F. Nori, and A. F. Kockum, *Simple preparation of bell and greenberger-horne-zeilinger states using ultrastrong-coupling circuit qed*, *Phys. Rev. A* **98**, 062327 (2018).

[42] S.-f. Qi and J. Jing, *Generating noon states in circuit qed using a multiphoton resonance in the presence of counter-rotating interactions*, *Phys. Rev. A* **101**, 033809 (2020).

[43] S. Gröblacher, K. Hammerer, M. R. Vanner, and M. Aspelmeyer, *Observation of strong coupling between a micromechanical resonator and an optical cavity field*, *Nature (London)* **460**, 724 (2009).

[44] E. Verhagen, S. Deléglise, S. Weis, A. Schliesser, and T. J. Kippenberg, *Quantum-coherent coupling of a mechanical oscillator to an optical cavity mode*, *Nature (London)* **482**, 63 (2012).

[45] J. Bochmann, A. Vainsencher, D. D. Awschalom, and A. N. Cleland, *Nanomechanical coupling between microwave and optical photons*, *Nat. Phys.* **9**, 712 (2013).

[46] M. Aspelmeyer, T. J. Kippenberg, and F. Marquardt, *Cavity optomechanics*, *Rev. Mod. Phys.* **86**, 1391 (2014).

[47] J.-M. Pirkkalainen, S. Cho, F. Massel, J. Tuorila, T. Heikkilä, P. Hakonen, and M. Sillanpää, *Cavity optomechanics mediated by a quantum two-level system*, *Nat. Commun.* **6**, 6981 (2015).